Designing Airfoils using a Reference Point based Evolutionary Many-objective Particle Swarm Optimization Algorithm

Upali K. Wickramasinghe, Robert Carrese and Xiaodong Li

Abstract— In this paper, we illustrate the use of a reference point based many-objective particle swarm optimization algorithm to optimize low-speed airfoil aerodynamic designs. Our framework combines a flexible airfoil parameterization scheme and a computational flow solver in the evaluation of particles. Each particle, which represents a set of decision variables, is passed through this framework to construct and evaluate the airfoils and assign fitness. We used the baseline NLF0416 airfoil to obtain aspiration values, which are used to define the reference point. This reference point guides the swarm towards the preferred region of the objective landscape to find solutions of interest to the decision maker. The proficiency of the algorithm is highlighted by monitoring convergence and spread of solution using a hyper-volume calculation scheme suitable for user-preference based evolutionary many-objective algorithms. The results comparing the reference point based approach with a standard unguided non-dominated sorting based approach shows that the guided algorithm performs better in this many-objective problem instance. Final solutions found from the reference point based algorithm reveal an evident improvement over the NLF0416 airfoil across all operating conditions.

I. INTRODUCTION

Shape optimization is considered across a wide range of engineering disciplines. Modifications to existing or new geometries are performed iteratively to conform to the best performing shape for a given objective or requirement. In the aerospace industry, the process of aerodynamic shape optimization to low speed Unmanned Aerial Vehicles (UAV) is critical during all phases of design [1]. The recurring strategy in aerodynamic shape optimization [2], [3], [4] is the integration of three distinct modules:

- Geometry parameterization model
- Computational flow solver
- Efficient search engine

Of particular importance to aerodynamic design, are bodies of which, the force parallel and opposite to the direction of motion (*drag*) is significantly smaller in magnitude to the force component acting normal to the direction of motion (*lift*). A discipline which has benefited greatly from optimization theory in the recent past is airfoil design [5]. Airfoils denote the cross-section of any three-dimensional lifting surface, such as the main wing. Subsonic forces for main wing airfoil sections arise from surface pressure and air viscosity. The pressure difference of the upper and lower

surface produces the resultant lift force required to maintain level flight for a given operating condition. The location where the resultant lift force acts generates a moment, which governs the magnitude and direction of the pitch inclination. Drag is comprised of both pressure and viscous components, the latter dominating in subsonic flight. Viscosity of the flow in the immediate vicinity of the surface (*boundary layer*) generates surface shear stress from which drag is derived.

For the stipulated operating condition, deviations to the airfoil geometry will result in variations to the pressure and shear stress distributions, which in turn alter the force values. In shape optimization, an algorithm is used to determine the necessary perturbations to the airfoil geometry in order to reduce the desired force (*objective*). In airfoil design and analysis, it is customary to express these forces as scalar coefficients. It follows, that for a geometrically similar airfoil at a given flow incidence angle (α), the lift (C_l), moment (C_m) and drag (C_d) are a function of:

$$[C_l, \ C_m, \ C_d] = f\left(\alpha, \mathrm{Re}, \mathrm{Ma}\right) \qquad (1)$$

where, the Reynolds number (Re) is the dimensionless ratio of the intertial forces to viscous forces and quantifies their respective relevance for a given operating condition. The Mach number (Ma) is a measure of the air velocity against the speed of sound. There are several methods that can be used to compute these coefficients, that vary in accuracy and computational expense. The solver employed in this paper follows the work in [6]. Dependent on the mission phase, one of these force coefficients is generally treated as the objective function, while providing some constraints on the other values. For example in cruise, designers attempt to reduce the drag coefficient at the required lift coefficient to maintain steady flight for fuel economy. However during take-off, emphasis is placed on maximizing the lift coefficient [2].

Despite advantages at one flight condition, a good design is one that exhibits optimal aerodynamic performance over a range of flight conditions and mission segments. Traditional concepts of developing platforms for single mission requirements have resulted in a large number of UAV with difficulties in operation and support. Future mission requirements have confirmed that the single mission design concept is neither operationally nor financially feasible [1]. Alternatively, a multi-mission platform is regarded as a viable design concept to address the issues with the current UAV fleet. Present UAV platforms are plagued with performance restrictions and operations outside the intended design envelope are not permissible. For example, long endurance platforms are optimized for slow speed operations at low Reynolds number

Upali K. Wickramasinghe and Xiaodong Li are with the School of Computer Science and Information Technology, RMIT University, Melbourne, VIC 3001, Australia (phone: +61 3 9925 2348; email: uwickram@cs.rmit.edu.au and xiaodong@cs.rmit.edu.au).

Robert Carrese is with the School of Aerospace Mechanical and Manufacturing Engineering, RMIT University, Bundoora, VIC 3083, Australia (phone: +61 3 9925 6187; email: robert.carrese@rmit.edu.au).

operation. Performing high g-force manoeuvres with these platforms would result in suboptimal performance [1]. The current design philosophy focuses on designing UAV airfoils for multi-mission capabilities.

Gradient based methods have been applied for single-mission airfoil designs [7], [8], but the search process may converge prematurely due to the multi-modal landscape [3]. Evolutionary Algorithms (EA) have thus received much attention because they are less prone to get stuck in local optimum solutions [5]. The evolution of population-based heuristics to address many-objectives is yet another step forward in providing a multi-mission operational spectrum to UAV platforms. In this paper, a reference point based Evolutionary Many-objective Optimization (EMO) algorithm is used to explore the search-space to obtain optimal designs for disparate conditions. The Decision Maker (DM) provides a reference point in the objective-space to guide the EMO algorithm towards solutions which are of most interest. The reference point based Differential Evolution (DE) and Particle Swarm Optimization (PSO) algorithm – MDEPSO, described in [9] is used to explore the many-objective search-space. Recently the use of preference mechanisms has been gathering interest in the EMO community because of their ability to handle problems of more than three-objectives successfully. Multi-mission airfoil designs are a problem domain consisting of such many-objectives. A DM of this domain can guide EMO algorithms to obtain solutions which are useful than trying to search the entire Pareto front. The PSO framework described in [9] shows that using a preference mechanism like reference points, EMO algorithms can efficiently locate solutions without any need for dominance comparisons. PSO algorithms are well suited to be guided by the reference points because of their design philosophy on *following a leader*.

The paper is organized as follows. Section II discusses the adopted airfoil parameterization scheme. These parameters are used as the decision variables for this study. Section III presents the six-objective problem domain. The reference point used in this problem is the benchmark low-speed NLF0416 airfoil. The MDEPSO algorithm is described in Section IV. We next present an extension to the Hyper-Volume (HV) metric to propose a suitable performance metric for user-preference EMO algorithms. We use this HV metric to illustrate the performance of the reference point based EMO algorithm against a traditional dominance based PSO algorithm in Section VI. This section will also present the improved airfoil geometries obtained from the EMO framework. Finally, in Section VII, we present our conclusions and avenues for future research.

II. AIRFOIL SHAPE PARAMETERIZATION

Airfoil geometry has been represented using a variety of methods [10]. The selection of the parameterization scheme is an important contributing factor to the efficiency of the algorithm since it will define the objective landscape and the topology of the design space [5], [10]. Furthermore, certain parameterization techniques are suited to specific forms of
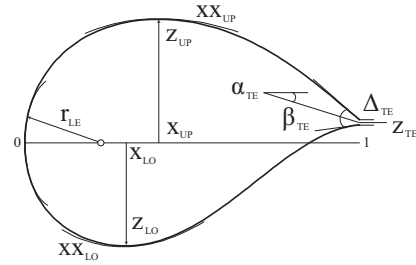

Fig. 1. PARSEC method for airfoil parameterization

optimization. The development of efficient parameterization models has therefore been given significant attention, to increase the flexibility of geometrical control with a minimum number of design variables.

A. PARSEC Method

A common method for airfoil shape parameterization is the PARSEC method [11]. It has the advantage of strict control over important aerodynamic features, and it allows independent control over the airfoil geometry for imposing shape constraints.

Illustrated in Figure 1 are the basic eleven parameters that are used to completely define the profile geometry. They include the leading edge radius (r_{LE}), the upper and lower crest locations ($x_{UP}, z_{UP}, x_{LO}, z_{LO}$) and curvatures ($xx_{UP}, xx_{LO}$), trailing edge coordinate (z_{TE}) and thickness (Δ_{TE}), trailing edge direction (α_{TE}) and wedge angle (β_{TE}). In this study, the variable $\Delta_{TE} = 0$. Thus, blunt trailing edge sections are not considered and the number of search-space (decision-space) dimensions is reduced to ten. The optimizer perturbs the geometrical variables to generate different airfoil shapes, based on the performance rating provided by the flow solver.

B. Variable boundaries

Providing feasible boundaries for the PARSEC parameters is yet another contributing factor to increasing efficiency of the optimization architecture. A certain class of airfoils does not provide favourable aerodynamic performance under all flight conditions. With knowledge of the occurring flow-field, the PARSEC parameters may be restricted to conform to a specific family of airfoils. This is achieved through inverse mapping of benchmark profiles that have been developed (either by experimental or computational methods) to perform favourably in low-speed flow conditions [12]. These include representative profiles of the NLF series and the NACA/NASA series [13]. Defining the airfoil boundaries through inverse mapping as opposed to arbitrarily selecting boundaries is advantageous to omit poorly performing areas of the design space. The upper and lower values for the parameter boundaries are shown in Table I.

III. PROBLEM DEFINITION

In this study, emphasis is placed on the ability to locate feasible solutions in a many-objective environment. Six objectives have been formulated for this problem, which

TABLE I
PARSEC DECISION VARIABLE RANGES

Decision Variable	Upper Bound	Lower Bound
r_{LE}	0.0055	0.0215
α_{TE}	0.3580 (-)	0.0230
β_{TE}	0.0200	0.2600
x_{UP}	0.2875	0.5345
z_{UP}	0.0880	0.1195
xx_{UP}	1.0300 (-)	0.4200 (-)
x_{LO}	0.3060	0.5075
z_{LO}	0.0650 (-)	0.0500 (-)
xx_{LO}	0.0490 (-)	0.8205
z_{TE}	0.0200 (-)	0.0200
Δ_{TE}	0	0

relate to various mission segments and requirements. The ten PARSEC parameters constitute the decision variables. Lift constraints are satisfied explicitly, by letting the flow solver determine the angle of incidence that generates the desired lift. Geometrical constraints are inherent within the defined PARSEC variable boundaries.

The reference point airfoil selected for this application is the NLF0416 airfoil [12]. It is considered a benchmark profile for low-speed applications because the experimental data are available. The NLF0416 is a 16% thick airfoil designed for a moderate lift coefficient in cruise conditions. It has a relatively high upper-surface curvature to maintain favourable pressure gradients for laminar flow control, whilst providing increased maximum lift values for manoeuvring due to the highly cambered aft section. The NLF family is the product of years of prior research in subsonic airfoil aerodynamics.

A. Software Analysis Tool

The software tool XFOIL [6] is selected as the computational flow solver. XFOIL is a viscous-inviscid iterative software code which does not require any prior mesh preparation. The inviscid pressure distribution is modelled using a linear vortex strength distribution. Viscous effects and the development of the laminar-turbulent boundary layer are modelled using empirical integral boundary layer theory. XFOIL provides relatively accurate results for subsonic airfoil analysis rapidly. Such software is predominately used in screening processes during preliminary design as a precursor to detailed modelling and wind-tunnel simulations.

B. Objective functions

The formulated objectives cover a range of mission segments and would be typical of multi-mission UAV requirements. Here, we formulate all the objectives to be minimized. It is essential that the airfoil exhibit low drag values during cruise flight. For the first objective, minimization of the drag coefficient at an operating lift coefficient of 0.5 is required. The Reynolds number and Mach number are fixed at 4×10^6 and 0.3 respectively. This objective is represented as:

$$f_0 = C_d \text{ at } C_l = 0.5, \text{ Re} = 4 \times 10^6, \text{ Ma} = 0.3 \quad (2)$$

It is of equal importance that the airfoil obtain a high maximum lift-to-drag ratio for climbing, as well as increased

flight endurance. Maximum endurance is a pre-requisite for UAV which are expected to perform automated missions for an extensive period. For each candidate solution, the incidence angle is floated to determine the minimum drag-to-lift ratio. The lift-to-drag objective is given as:

$$f_1 = C_d / C_l^{3/2} \text{ at } \text{Re} = 4 \times 10^6, \text{ Ma} = 0.3 \quad (3)$$

Providing a reduced drag design during cruise conditions generally occurs at the expense of a highly aft cambered airfoil section which results in excessive pitching moments. Formulating the objective to minimize the zero-lift pitching moment coefficient is desirable for stability and control. The incidence angle which corresponds to zero-lift generation (α_0) is determined. The pitching moment at this point (C_{m_0}) is recorded. Therefore, the objective to reduce the drag is:

$$f_2 = C_{m_0}^2 \text{ at } \text{Re} = 4 \times 10^6, \text{ Ma} = 0.3 \quad (4)$$

The preceding objectives are deemed as sufficient to address optimal cruise performance. The UAVs are however also required to perform manoeuvres at cruise without the risk of stall. The objective to maximize the highest possible lift coefficient $(C_{l_{\max}})$ before stall occurs is given as:

$$f_3 = 1/C_{l_{\max}}^2 \text{ at } \text{Re} = 4 \times 10^6, \text{ Ma} = 0.3 \quad (5)$$

During descent and approach, a high lift value is beneficial as it constitutes towards an increased lift-induced drag, which is essential for landing. Here the angle of incidence is fixed at $5°$, which is regarded as a typical incidence angle during approach flight. Thus the objective for high lift is given as:

$$f_4 = 1/C_l^2 \text{ at } \alpha = 5°, \text{ Re} = 2 \times 10^6, \text{ Ma} = 0.15 \quad (6)$$

Providing optimal performance in the approach condition should not be at the expense of massive flow separation or leading-edge boundary layer transition (x_{tr}). In this case, it is sought to maintain a smooth flow-field during approach flight by maximizing the laminar portion of the upper surface of the airfoil. Therefore, the objective to obtain a maximum boundary layer is:

$$f_5 = 1/x_{tr} \text{ at } \alpha = 5°, \text{ Re} = 2 \times 10^6, \text{ Ma} = 0.15 \quad (7)$$

With the formulated objectives, mission phases such as cruise/endurance, approach/descent and manoeuvring have been addressed. Further objectives may be formulated which consider take-off, multi-point cruise etc., but are beyond the current scope of this study. The array of aspiration values representing the NLF0416 airfoil are given as [0.00516, 0.00606, 0.00982, 0.30806, 0.92314, 0.65460] [12].

IV. REFERENCE POINT BASED MDEPSO

We use the reference point based MDEPSO algorithm as described in [9] to obtain solutions for the airfoil design problem. The MDEPSO algorithm has been shown to be effective in finding solutions in difficult multi-modal many-objective problem instances [14]. The unique feature of this PSO algorithm is that the leaders are generated using a DE rule rather than selecting particles as leaders from the population. The basic outline of the algorithm is given as:
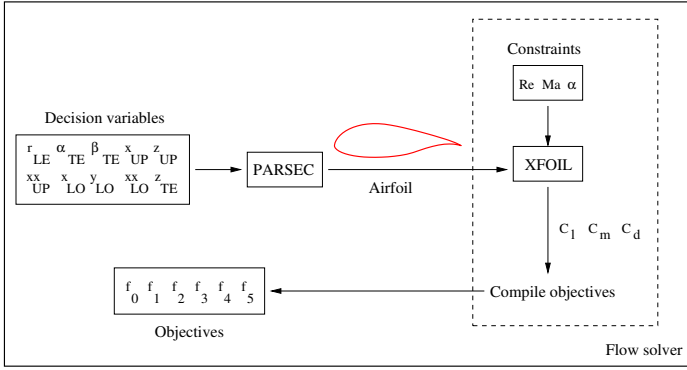
Fig. 2. Evaluation framework

- **Step 1: Initialize the particles**
  A population of size N is first initialized. Here, a particle's 10 decision variables (position vector $\vec{x} = [x_0, \ldots, x_9]$) are initialized using (8).

  $$rand(0.0, 1.0) \times (UB - LB) + LB \qquad (8)$$

  where, $rand(0.0, 1.0)$ represents a random number generated uniformly between $[0.0, 1.0]$. LB and UB are the lower-bounds and upper-bounds respectively of the decision variables. The velocity is initialized to a random value in the interval $[0, UB - LB]$. The personal best of an individual is set to its current position. Half of the population's direction is reversed by setting the velocity to negative according to a coin toss. The particles' position vectors are used to generate the respective candidate airfoil shapes. These airfoils are subsequently analyzed by XFOIL to assign fitness values. This process is illustrated in Figure 2.
  After initialization, each particle's distance metric value is assigned using the reference point $\vec{\bar{z}}$ as:

  $$dist(\vec{x}) = \max_{i=0,\ldots,5} \{ w_i(f_i(\vec{x}) - \bar{z}_i) \} \qquad (9)$$

  where, $\vec{\bar{z}} = [\bar{z}_0, \ldots, \bar{z}_5]$ is the reference point and $\vec{w} = [w_0, \ldots, w_5]$ is a set of weights. f_i is the ith objective function. The DM can assign values for weights, which represent any bias towards that objective. In this problem we did not use any bias.

- **Step 2: Obtain leaders to guide the population**
  Leaders are generated using the DE rule described in [9]. These leaders are sorted according to the distance metric given by (9). To control the spread of solutions the $\delta(> 0)$ value is used to define the notion of *outranking* [9]. A small value for δ represents a smaller spread, while a large value will give a larger spread. In our experiments $\delta = 0.05$. A subset of the sorted leaders (for example 10% of the population) closest to the preferred region is chosen to guide the population.

- **Step 3: Move the particles**
  Each particle chooses its leader randomly from the sorted set of potential leaders. Using this leader as the

global best the particle updates its velocity ($\vec{v}_i$) and position ($\vec{x}_i$) according to the PSO update rules from time t to $t + 1$ as:

$$\vec{v}_i(t+1) = \chi(\vec{v}_i(t) + \phi_1(\vec{p}_i(t) - \vec{x}_i(t)) + \phi_2(\vec{p}_g(t) - \vec{x}_i(t))) \qquad (10)$$

$$\vec{x}_i(t+1) = \vec{x}_i(t) + \vec{v}_i(t) \qquad (11)$$

here, $\vec{p}_i$ is the particle's personal best position so far. ϕ_1 and ϕ_2 are random numbers generated uniformly between $[0, \frac{\varphi}{2}]$. φ is a constant equal to 4.1 [15]. χ is the so called *constriction factor*, which is used to prevent a particle from exploring too far into the search-space. χ is normally set to 0.7298, which is calculated according to $\frac{2}{|2-\varphi-\sqrt{\varphi^2-4\varphi}|}$ [15].

- **Step 4: Update the particles' personal bests**
  Each particle updates its personal best according to the distance metric given in (9).

- **Step 5: Obtain the particles to move to the next iteration**
  The population of N particles at the beginning of the iteration is combined with the N updated particles to create a population of size $2N$. This $2N$ population is sorted according to (9) to obtain a population of size N closest to the preferred region. These N particles will survive to the next iteration.

The steps 2 to 5 are repeated until the maximum number of iterations is reached.

V. PERFORMANCE METRIC

There are several popular performance metrics used to determine the convergence and spread of solutions in the EMO literature, which are described in [16]. However, these metrics are suitable only for problems with known Pareto fronts. In the airfoil design problem the true Pareto fronts are unknown, thus a performance metric which does not rely on the true Pareto front is required. The Hyper-Volume (HV) metric [17] can be used as performance metric because it does not rely on the knowledge of the true Pareto front. The HV metric provides a single measurement to assess both the convergence and spread of solutions. Theoretical results in [18] show that, when a solution set dominates another solution set, the HV metric yields better values for the dominant set of solutions. However, the standard HV calculation procedure has to be modified to include only the solutions points within the preferred regions, not the entire Pareto front.

A. The Hyper-Volume metric

The HV metric gives the total volume bounded by the solutions points on the solution front and a selected point in the objective-space. This selected point is usually called the *nadir point*. At the nadir point, all objectives are at their worst values simultaneously [19]. The nadir point $\vec{x}_{nad}$ is given as $\vec{x}_{nad} = [f_0^{nad}(\vec{x}), \ldots, f_{M-1}^{nad}(\vec{x})]$, where $f_i^{nad}(\vec{x}) = \max_{j=1\ldots pop\_size} \{ f_i(\vec{x}_j) \}$.

The formal definition of HV metric according to [20] is the Lebesgue measure (Λ) of the union of all hypercubes a_i defined by a solution point $\vec{b_i} \in B$ (B is the population of all the non-dominated solution points), and the nadir point $\vec{x}_{nad}$, given in (12). $\vec{x} \prec \vec{x}_{nad}$ denotes $\vec{x}$ dominates $\vec{x}_{nad}$. The HV value is the sum of all the volumes:

$$hv(B) = \Lambda(\{\bigcup_i a_i | \vec{b_i} \in B\}) = \Lambda(\bigcup_{\vec{b_i} \in B} \{\vec{x} | \vec{b_i} \prec \vec{x} \prec \vec{x}_{nad}\}) \tag{12}$$

In experiments where multiple runs are required to obtain an average HV value, the population will be the sum of all the final non-dominated individuals from each run combined together. The nadir point is computed from this combined population, and then will be used to obtain the HV value for each run. This method ensures a consistent nadir point for all runs of the experiment.

When comparing two EMO algorithms, the one which gives a larger HV value is considered to be better. The volume calculated by this metric gives a measure on both the spread and the closeness of the solutions to the Pareto front.

B. HV metric for user-preference EMO algorithms

The goal of user-preference EMO algorithms is to locate solutions in the preferred regions. Therefore, the HV calculation should also incorporate this information to make it suitable for such algorithms. We propose to exclude the solutions points outside the preferred regions so that the nadir point used for the HV calculation lies within the preferred region. This will favour the HV calculation towards algorithms that converge onto the preferred regions.

We propose to extend the standard HV metric in the following manner for one preferred region. The experiments in this paper have only one preferred region, defined by the given reference point.

- **Step 1: Obtain the solution point closest to the ideal point**
  First, all the final solutions points from every run of each algorithm is combined to make a single population. Next, the Euclidean distance is calculated for each solution point in this population from the ideal point. The solution point with the lowest Euclidean distance is selected to define a volume.

- **Step 2: Define a volume for HV calculation**
  A volume is defined around the solution point with the lowest Euclidean distance. As seen in Figure 3, for a two-objective minimization problem the ideal point is $(0.0, 0.0)$. The DM can provide value to define the volume. We represent this value as δ', so that a volume is defined having $2\delta'$ for each objective. The DM can adjust this δ' value such that a sufficient number of solution points lie within the defined volume.

- **Step 3: Filter solutions points and calculate the HV**
  Solution points from the final set of solutions (from all algorithms and runs in consideration) are removed if
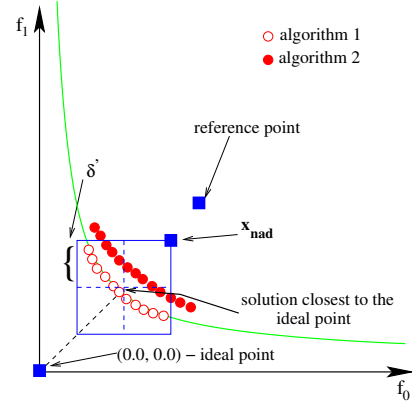

Fig. 3. Defining a volume around the closest solution point to the ideal point
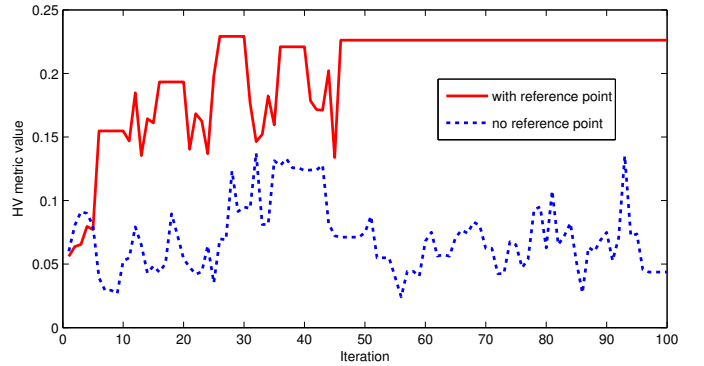

Fig. 4. HV values at each iteration

they reside outside this common volume. The remaining solution points are used to obtain the nadir point, which will be located within the defined volume. The calculation of the HV values for each run of each algorithm is done using this common nadir point and solution points within the volume.

VI. EXPERIMENTS

To perform a comparative analysis of the reference point based approach against the traditional dominance based approach in airfoil designs we used the original MDEPSO algorithm described in [14] and the reference point based algorithm. Both algorithms used a population of size 100 for 100 iterations. The evaluation process of individuals are computationally expensive, due to the complex nature of the matrix operations within the analysis process. We decided on these parameter values for the EMO algorithm as a trade-off for the heavy time consumption. Initial results indicated that $10,000$ evaluations take about 36 hours on a $2.3GHz$ dual-core CPU machine. $CR = 0.2$ and $F = 0.4$ was used for the DE operator in MDEPSO. We used a spread value of $\delta = 0.05$ for the reference point approach. The results shown here are an average of 10 independent runs.

A. Convergence and spread of solutions

Figure 4 illustrates the average HV values at each iteration of the runs. We used $\delta' = 0.5$ to define a volume in the
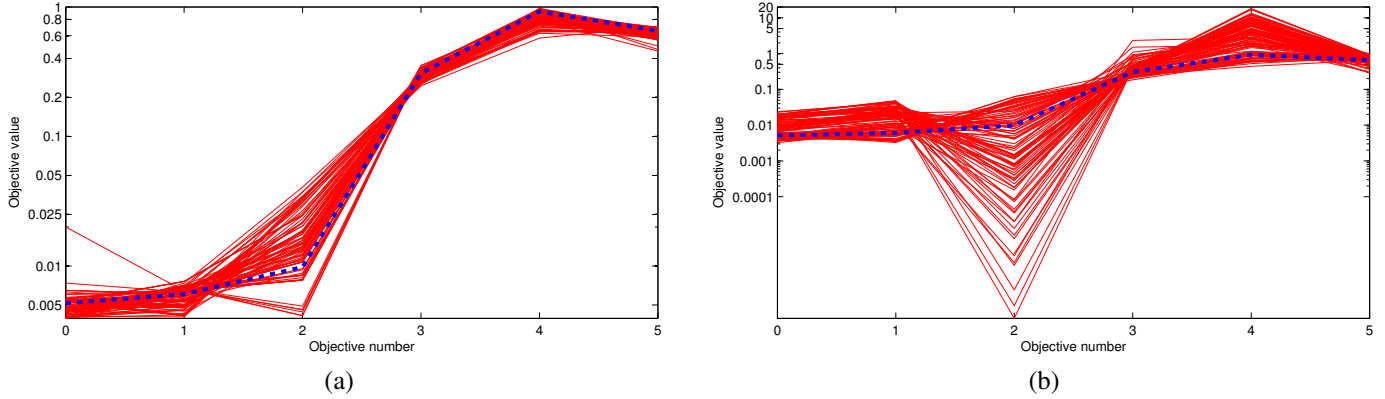
Fig. 5. Final solutions obtained on MDEPSO: (a) with reference point; (b) without reference point (Each line represents a solution point, where the intersection at the objectives axis represents the value for that objective. The bold dashed line is the reference point.)

preferred region, so that at least 90% of the particles of the algorithm, which has better convergence, is selected. Then as described in Section V-B a nadir point was selected and the HV values at each iteration was calculated. To promote diversity in the algorithm, particles will follow the leaders generated by the DE step in the original MDEPSO algorithm from time to time, rather than following leaders closest to preferred regions. These incidents can be seen by the abrupt changes of the HV values. This is due to the fact that particles might move away from the preferred region to explore the search-space and avoid getting stuck at local optima. It is clear from the results that as the iterations progresses the reference point based algorithm converges better than the dominance based algorithm. The results also show that the reference point based algorithm has converged to an optimum at about iteration 50, while the dominance based algorithm fails to converge even after the maximum number of iterations have been reached. These results show that the reference point based MDEPSO algorithm performs much better in a six-objective problem instance as opposed to a standard non-dominance sorting based approach.

Figure 5 shows the solution points obtained from best runs of each algorithm. Here, the reference point is given as the *dashed* line, while the solid lines represent the candidate solutions. It is clear that the reference point based algorithm converges better in all objectives than the other algorithm. We'll next present an analysis of the designs for each operating condition (objective) separately, which shows that the reference point based algorithm provides better solutions than the benchmark NLF0416 design.

B. Final designs

From our perspective, the airfoil which exhibits the most feasible compromise between all objectives is considered the most preferred solution. In this case, the *preferred solution* is the one which has the minimum distance metric. It follows that the candidate solution, the closest compromising solution, to the NLF0416 is the most improved design. The variation in airfoil geometry is shown in Figure. 6.

Consistent with low-speed airfoil design theory, the preferred solution has a relatively large leading edge radius,
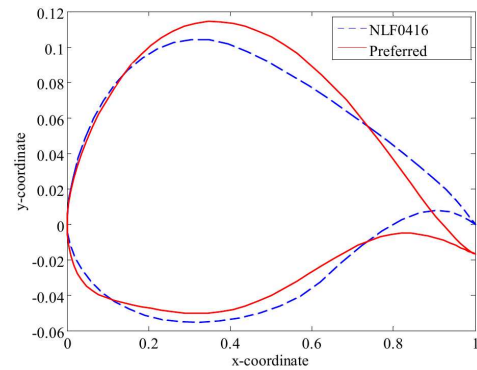

Fig. 6. Comparison of the preferred solution and the reference NLF0416 solution

which results in an approximately 16.5% thick airfoil. The upper surface is highly cambered, prolonging laminar flow during cruise. The lower surface is quite flat, which induces a lower moment value and is beneficial for stability. The airfoil has a highly cambered aft section for lift generation. The trailing edge is drooped and the wedge angle is significantly small. Further study has proven that the trailing edge wedge geometry may be impractical to manufacture. Additional constraints must be imposed on the design variables to restrict such geometries. The drooped trailing edge is essential to limit separation of the boundary layer, which results in lower drag values and less chaotic flow when generating increased lift. The function values of the preferred airfoil are listed in Table. II. Also tabulated are airfoils which exhibit the most optimal value for the respective objectives. It is observed that with a marginal increase in the objectives 0 and 3 compared to the NLF0416, an improvement of approximately 13%, 27% and 9% is obtained for the preferred solution for objectives 1, 4 and 5 respectively. Despite improvements in these objectives, the NLF0416 still exhibits greater stability characteristics with a 30% lower value in objective 2 over the preferred airfoil. Figure 7 feature the pressure coefficient distribution of the preferred airfoil against the NLF0416 for the cruise operating condition. The curve which predominantly has a negative pressure is the upper (suction)

TABLE II

Airfoil	Obj. 0	Obj. 1	Obj. 2	Obj. 3	Obj. 4	Obj. 5
NLF0416	0.00516	0.00606	0.00982	0.30806	0.92314	0.65460
Preferred	0.00536	0.00537	0.01281	0.31430	0.67285	0.59530
min Obj. 0	0.00407	0.00726	0.01713	0.28737	0.91924	0.64170
min Obj. 1	0.00408	0.00404	0.02883	0.30024	0.97161	0.62610
min Obj. 2	0.00559	0.00671	0.00413	0.33868	0.96098	0.57380
min Obj. 3	0.00412	0.00472	0.03984	0.23977	0.88731	0.70100
min Obj. 4	0.00604	0.00523	0.01968	0.27611	0.58638	0.64360
min Obj. 5	0.00536	0.00477	0.01145	0.32364	0.93441	0.45250

TABLE III

IMPROVEMENT OVER NLF0416 FOR RESPECTIVE OBJECTIVES

Airfoil	% Improvment
min (2)	21.1% for Obj. 0
min (3)	33.3% for Obj. 1
min (4)	57.9% for Obj. 2
min (5)	22.1% for Obj. 3
min (6)	36.5% for Obj. 4
min (7)	30.9% for Obj. 5

surface. Similarly, the lower (pressure) surface is denoted by the curve which is predominately experiencing positive pressure. The difference between these two curves yields the resultant force. Figure 8 shows that the pressure differences between the highest and lowest points of the x-coordinates are on average greater on the preferred airfoil compared with the NLF0416. This indicates that for the stipulated operating condition (objective 4) a greater lift is achieved (or a reduced inverse, as indicated in Table. II). Figures 9 and 10 feature the drag polar and lift curves. The drag polar demonstrates that for incidence angles up to $\alpha = 6°$, the preferred airfoil exhibits greater aerodynamic efficiency, as denoted by the reduced drag-to-lift ratio (corresponding to objectives 1 and 4). The lift curve of the preferred airfoil shows a consistently greater lift is achieved for values up to $\alpha \approx 7°$, after which boundary layer separation on the suction surface results in lower lift values. This phenomenon is validated by objective 3, which indicates a lower maximum lift (or higher inverse) is achieved compared with NLF0416.

Table II also demonstrates the improvement over the NLF0416 for solutions which exhibit minimum values for particular objectives. This is beneficial if the DM was inclined towards a particular objective, rather than a feasible compromise. It is observed that there is one solution which improves on the NLF0416 for at least one objective at a time. The percentage improvements for the respective objectives are shown in Table III.

VII. CONCLUSIONS

In this paper we illustrated the use of a reference point based many-objective PSO algorithm in the optimization of airfoil designs. This study described six conflicting objectives, which represents six operational conditions under which an airfoil design may be optimized. Using the
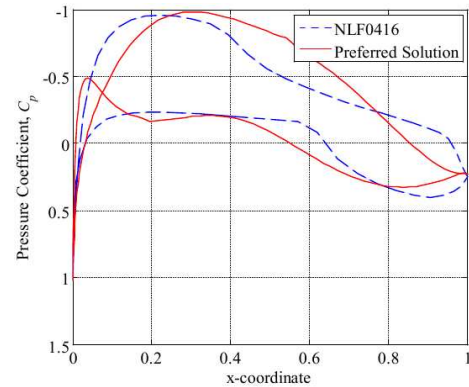

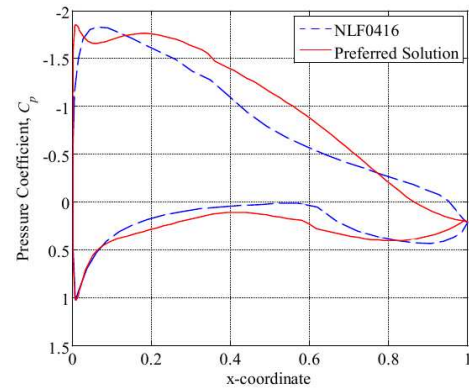Fig. 7. Pressure distribution, $C_l = 0.5$, M = 0.3, Re $= 4 \times 10^6$

Fig. 8. Pressure distribution, $\alpha = 5°$, M = 0.15, Re $= 2 \times 10^6$

NLF0416 airfoil as a reference design, we defined a reference point using the aspiration values of NLF0416 at each operating condition. The PARSEC method is used to define the shape of an airfoil using ten decision variables. The evaluation framework first creates an airfoil using the decision variables, then is given to the flow solver with explicit constraints, to obtain values for the lift (C_l), moment (C_m) and drag (C_d) coefficients. We have used XFOIL as the flow solver in this study. Using these coefficients, objectives are formulated to be minimization functions. The MDEPSO algorithm incorporates this evaluation framework to guide the particles towards the preferred region of the objective-space indicated by the reference point.
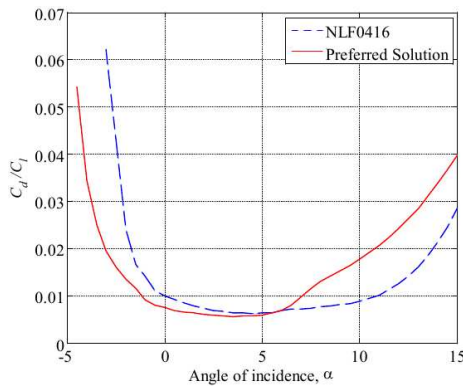
Fig. 9.   Drag to lift ratio polar, M = 0.15, Re = 2×10^6

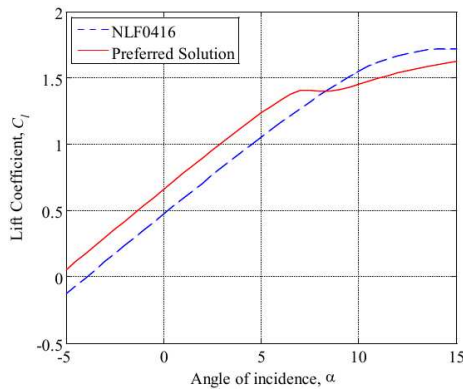
Fig. 10.   Lift coefficient curve, M = 0.15, Re = 2×10^6

The experimental results suggests that by using a reference point, the EMO algorithm is more effective and efficient in locating useful solutions than using a standard non-dominated sorting based approach. We have illustrated this feature using an HV metric suitable for user-preference EMO algorithms. This modified calculation of the HV metric takes into consideration only the solutions within the preferred region. This process of excluding solutions outside the preferred region defined by the DM is suitable for EMO algorithms which only concentrate on certain regions of the search-space. Our results also illustrate the improvements of the derived airfoils compared with the NLF0416 airfoil. We have also described the best solutions obtained for each operating condition (objective). The results show that using a population based approach the DM now has the ability to obtain airfoils that perform better in all operating conditions or on selected operating conditions, without requiring to re-run experiments with different parameter settings. This is a very useful feature of this approach, because the evaluation process in airfoil designs are computationally intensive.

We have found some shortcomings of the derived airfoils, which need to be fixed before the manufacturing process. In future we plan to incorporate more objectives to the evaluation framework, which will address these issues. We also plan to explore other problems where a similar evaluation process can be used within a user-preference EMO framework.

References

[1] M. S. Khurana1, A. K. Sinha, and H. Winarto, "Multi-mission re-configurable uav - airfoil optimization through swarm approach and low fidelity solver," in *Bristol International Unmanned Air Vehicle Systems*, 2009.

[2] D. Quagliarella and A. Vicini, "Viscous single and multicomponent airfoil design with genetic algorithms," *Finite Elements in Analysis and Design*, vol. 37, no. 5, pp. 365–380, 2001.

[3] M. S. Khurana1, H. Winarto, and A. K. Sinha, "Airfoil optimization by swarm algorithm with mutation and artificial neural networks," in *AIAA Aerospace Sciences Meeting Including The New Horizons Forum and Aerospace Exposition*, 2009.

[4] T. Ray and H. M. Tsai, "Swarm algorithm for single and multiobjective airfoil design optimization," *American Institute of Aeronautics and Astronautics (AIAA)*, vol. 42, no. 2, pp. 366–373, 2004.

[5] A. Keane and P. Nair, *Computational Approaches for Aerospace Design: The Pursuit of Excellence*.   John Wiley Sons, Ltd., 2005.

[6] M. Drela and M. B. Giles, "Viscous-inviscid analysis of transonic and low reynolds number airfoils," *American Institute of Aeronautics and Astronautics (AIAA)*, vol. 25, no. 10, pp. 1347–1355, 1987.

[7] J. R. A Jameson, "Control theory based airfoil design using the euler equations," *American Institute of Aeronautics and Astronautics (AIAA)*, 1994.

[8] W. K. Anderson and V. Venkatakrishnan, "Aerodynamic design optimization on unstructured grids with a continuous adjoint formulation," in *Institute for Computer Applications in Science and Engineering (ICASE) Technical Report Number TR-97-9*, 1997.

[9] U. K. Wickramasinghe and X. Li, "Using a distance metric to guide PSO algorithms for many-objective optimization," in *Genetic and Evolutionary Computation Conference (GECCO)*.   ACM, 2009, pp. 667–674.

[10] W. Song and A. J. Keane, "A study of shape parameterisation methods for airfoil optimisation," in *AIAA/ISSMO Multidisciplinary Analysis and Optimization Conference*, 2004.

[11] H. Sobieczky, "Parametric airfoils and wings," in *Notes on Numerical Fluid Mechanic*, ser. Numerical Fluid Mechanics.   Vieweg, 1998, pp. 71–88.

[12] D. S. Somers, "Design and experimental results for a natural-laminar-flow airfoil for general aviation applications," 1981.

[13] "UIUC airfoils coordinates database," http://www.ae.illinois.edu/m-selig/ads/.

[14] U. K. Wickramasinghe and X. Li, "Choosing leaders for multi-objective pso algorithms using differential evolution," in *Simulated Evolution And Learning (SEAL)*, ser. Lecture Notes in Computer Science, vol. 5361.   Springer, 2008, pp. 249–258.

[15] M. Clerc and J. Kennedy, "The particle swarm - explosion, stability, and convergence in a multidimensional complex space," *IEEE Transactions on Evolutionary Computation*, vol. 6, pp. 58–73, 2002.

[16] E. Zitzler, K. Deb, and L. Thiele, "Comparison of multiobjective evolutionary algorithms: Empirical results," *Evolutionary Computation*, vol. 8, pp. 173–195, 2000.

[17] J. Knowles and D. Corne, "On metrics for comparing non-dominated sets," in *IEEE Congress on Evolutionary Computation (CEC)*, 2002.

[18] M. Fleischer, "The measure of pareto optima applications to multi-objective metaheuristics," in *Evolutionary Multi-Criterion Optimization (EMO)*, ser. Lecture Notes in Computer Science, vol. 2632.   Springer, 2003, pp. 519–533.

[19] A. Messac and C. A. Mattson, "Normal constraint method with guarantee of even representation of complete pareto frontier," *American Institute of Aeronautics and Astronautic (AIAA) Journal*, 2004.

[20] M. Emmerich, N. Beume, and B. Naujoks, "An emo algorithm using the hypervolume measure as selection criterion," in *Evolutionary Multi-Criterion Optimization (EMO)*, ser. Lecture Notes in Computer Science, vol. 3410.   Springer, 2005, pp. 62–76.